

The advantages of sub-sampling and Inpainting for scanning transmission electron microscopy

Nigel D. Browning, Jony Castagna, Angus I. Kirkland, Amirafshar
Moshtaghpour, Daniel Nicholls, Alex W. Robinson, Jack Wells,
and Yalin Zheng

Published version information

Citation: ND Browning et al. The advantages of sub-sampling and Inpainting for scanning transmission electron microscopy. Appl Phys Lett 122, no. 5 (2023): 050501

DOI: [10.1063/5.0135245](https://doi.org/10.1063/5.0135245)

This article may be downloaded for personal use only. Any other use requires prior permission of the author and AIP Publishing. This article appeared as cited above.

This version is made available in accordance with publisher policies. Please cite only the published version using the reference above. This is the citation assigned by the publisher at the time of issuing the APV. Please check the publisher's website for any updates.

The advantages of sub-sampling and Inpainting for scanning transmission electron microscopy

Cite as: Appl. Phys. Lett. **122**, 050501 (2023); <https://doi.org/10.1063/5.0135245>

Submitted: 17 November 2022 • Accepted: 16 January 2023 • Published Online: 01 February 2023

 Nigel D. Browning, Jony Castagna,  Angus I. Kirkland, et al.



View Online



Export Citation



CrossMark

ARTICLES YOU MAY BE INTERESTED IN

[A perspective on physical reservoir computing with nanomagnetic devices](#)

Applied Physics Letters **122**, 040501 (2023); <https://doi.org/10.1063/5.0119040>

[Measurement and numerical analysis of intrinsic spectral linewidths of photonic-crystal surface-emitting lasers](#)

Applied Physics Letters **122**, 051101 (2023); <https://doi.org/10.1063/5.0135042>

[Emerging multi-frequency surface strain force microscopy](#)

Journal of Applied Physics **133**, 040901 (2023); <https://doi.org/10.1063/5.0131075>



Time to get excited.
Lock-in Amplifiers – from DC to 8.5 GHz

Find out more

Zurich Instruments

The advantages of sub-sampling and Inpainting for scanning transmission electron microscopy

Cite as: Appl. Phys. Lett. **122**, 050501 (2023); doi: [10.1063/5.0135245](https://doi.org/10.1063/5.0135245)

Submitted: 17 November 2022 · Accepted: 16 January 2023 ·

Published Online: 1 February 2023









View Online



Export Citation



CrossMark

Nigel D. Browning,^{1,2,a)}  Jony Castagna,^{3,4}  Angus I. Kirkland,^{5,6}  Amirafshar Moshtaghpour,^{1,5} 
Daniel Nicholls,¹  Alex W. Robinson,¹ Jack Wells,³ and Yalin Zheng^{3,7} 

AFFILIATIONS

¹Mechanical, Materials & Aerospace Eng., University of Liverpool, Liverpool L69 3GH, United Kingdom

²Sivananthan Laboratories, 590 Territorial Drive, Bolingbrook, Illinois 60440, USA

³Distributed Algorithms CDT, University of Liverpool, Liverpool L69 3GH, United Kingdom

⁴UKRI-STFC Hartree Centre, Daresbury Laboratory, Warrington WA4 4AD, United Kingdom

⁵Rosalind Franklin Institute, Harwell Science and Innovation Campus, Didcot OX11 0QS, United Kingdom

⁶Department of Materials, University of Oxford, Oxford OX2 6NN, United Kingdom

⁷Department of Eye & Vision Sciences, University of Liverpool, Liverpool L7 8TX, United Kingdom

^{a)} Author to whom correspondence should be addressed: nigel.browning@liverpool.ac.uk

ABSTRACT

Images and spectra obtained from aberration corrected scanning transmission electron microscopes (STEM) are now used routinely to quantify the morphology, structure, composition, chemistry, bonding, and optical/electronic properties of nanostructures, interfaces, and defects in many materials/biological systems. However, obtaining quantitative and reproducible atomic resolution observations from some experiments is actually harder with these ground-breaking instrumental capabilities, as the increase in beam current from using the correctors brings with it the potential for electron beam modification of the specimen during image acquisition. This beam effect is even more acute for *in situ* STEM observations, where the desired outcome being investigated is a result of a series of complicated transients, all of which can be modified in unknown ways by the electron beam. The aim in developing and applying new methods in STEM is, therefore, to focus on more efficient use of the dose that is supplied to the sample and to extract the most information from each image (or set of images). For STEM (and for that matter, all electron/ion/photon scanning systems), one way to achieve this is by sub-sampling the image and using Inpainting algorithms to reconstruct it. By separating final image quality from overall dose in this way and manipulating the dose distribution to be best for the stability of the sample, images can be acquired both faster and with less beam effects. In this paper, the methodology behind sub-sampling and Inpainting is described, and the potential for Inpainting to be applied to novel real time dynamic experiments will be discussed.

Published under an exclusive license by AIP Publishing. <https://doi.org/10.1063/5.0135245>

I. INTRODUCTION

In a standard scanning pattern used for scanning transmission electron microscopes (STEM) and many other instruments, the scan system works by moving the beam from left to right across a single row with a dwell time for each pixel in that row (Fig. 1). At the end of the row, the beam flies back to the left-hand side, moves down one pixel, and then completes a row again [this is like the way a traditional typewriter works or an older cathode ray tube (CRT) television]. After the flyback, the beam typically has a longer dwell time at the left-edge to allow for any hysteresis in the scan to damp out and the left-edge of

the scan to be aligned at the same location for each row. This form of scanning is known to present difficulties with beam damage, particularly on the left-hand edge of the raster, and this has led to alternative spiral scanning approaches^{1,2} to extract higher resolution images with less beam damage.

The beam size in the STEM is the same regardless of the magnification of the image, which can be as small as ~ 0.1 nm for a Cs-corrected STEM.^{3,4} In a low magnification image, therefore, the area of the scan is large, and the pixel size is correspondingly much larger than the size of the beam. For example, for the Cs-corrected

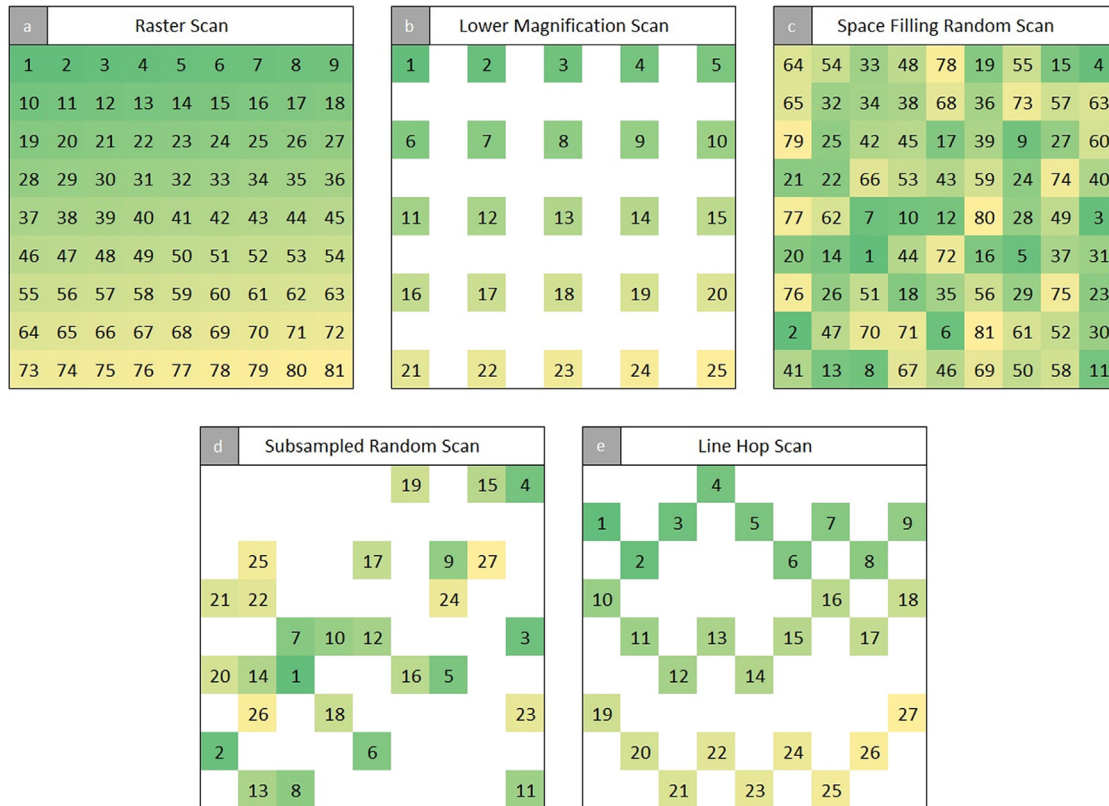


FIG. 1. Examples of various scanning patterns in a 9×9 grid. Number and color indicate scanning order. (a) Raster scanning is the traditional method of scanning in STEM. (b) Down sampling akin to low magnification image acquisition. (c) Space filling random scanning has been shown to reduce beam damage in beam sensitive samples.¹⁰ (d) and (e) Two scanning patterns possible using probe sub-sampling; sub-sampled random scanning and sub-sampled line hop (i.e., random walk) scanning at 33.3% sampling ratio.

STEM above, in a 1000×1000 -pixel scan covering $1 \times 1 \text{ mm}^2$, the pixel size is $1 \mu\text{m}$, i.e., $1000\times$ the size of the beam. To achieve atomic resolution in STEM, the magnification of the microscope is increased to the point where the pixel size approaches atomic separation, i.e., $\sim 0.1\text{--}0.5 \text{ nm}$. In the highest resolution images, the magnification is turned up to a level where the pixel size is actually much smaller than the probe size, leading to an oversampled image where beam damage is prevalent.⁵

When a STEM is at low magnification, beam damage is not a critical issue, as the distance between beam locations is very large, and the likelihood that the scan hits exactly the same location in successive sweeps is very small—damage can still occur, but it is below the scale of the image resolution. It is only when the beam and pixel size start to converge that the damage becomes serious, and this is, of course, the condition for the highest spatial resolution images. If we think about the problem from the perspective of overlapping beam positions and their effect on the measurable damage, then it is clear that if we can increase the spacing of the beam positions at high magnification, then we will be able to avoid/reduce the beam damage problem that plagues high resolution scanning electron microscope (SEM)/STEM (Fig. 1). This reduction in beam damage effects is actually what has been seen in cases where expanding the time and space between measurements

reduces damage.^{6–12} Of course, the issue with this “sparse sampling” approach is that we would then need a means to reconstruct the full image from the sub-sampled acquisition. As the quality of the image then would depend on how many pixels were included, the optimal sampling would be defined as where beam damage is minimized while the reconstruction quality is maximized. We note here that the recent development of the Moiré STEM achieves atomic resolution images from a lower magnification image (i.e., sub-sampled scan) with reduced dose by utilizing a geometrical interference effect between the STEM beam and the sample lattice.^{13–15} This methodology represents a special case, i.e., where the sample geometry is known and an atomic resolution image is desired, of the general sub-sampling approaches and reconstructions described in the remainder of this manuscript.

II. SPARSE SAMPLING AND RECONSTRUCTION FROM A SINGLE IMAGE

As we can see from Fig. 1, it is possible to obtain a sub-sampled scanned image by using both a set of “random” beam positions and a “random walk” or “line-hop” scan. Practically, the line-hop approach is easier to implement on standard electron microscopes as it avoids much of the hysteresis issue present in conventional scanning systems, permitting the system to run at the fastest possible speed¹¹

(more advanced electrostatic deflection systems can avoid this hysteresis⁵ and use the full benefit of a truly random scan). The key challenge for all sub-sampling methods is to reconstruct the sub-sampled image. Compressive sensing^{16,17} is a method of efficient signal acquisition and reconstruction via the solving of a set of undetermined linear equations. Like traditional image compression techniques, it relies upon the fact that given an appropriate coordinate system (or “Dictionary”), complex high dimensional signals such as an image can be expressed within a margin of error by a potentially much smaller set of parameters, describing a linear combination of signal patterns with their respective scalar coefficients.^{18,19} The goal for any image reconstruction is to form a complete signal (with the smallest error) from as few measurements as possible.^{20,21}

Traditional image inpainting methods rely on a dictionary learning algorithm such as the method of optimal directions (MOD)²² or K-SVD²³ to form a dictionary of representative signal patterns from a fully sampled image, which via a sparse linear combination with

corresponding scalar coefficients can closely represent any given patch (smaller segment) of the image. This dictionary, along with a now sub-sampled version of the same image, may then be passed to a sparse pursuit algorithm to solve the following system of equations (for each i th overlapping patch of the image):

$$\mathbf{v}_i = \Phi_i \cdot (\mathbf{D}\alpha_i + \epsilon_i), \quad (1)$$

$$\hat{\mathbf{x}}_i = \mathbf{D}\alpha_i, \quad (2)$$

where $\mathbf{v}_i \in \mathbb{R}^n$ is the measured (sub-sampled) signal subject to noise $\epsilon_i \in \mathbb{R}^n$, $\Phi_i \in \{0, 1\}^{n \times n}$ is the binary sensing matrix (or “mask,” determining the locations of missing pixels), and $\hat{\mathbf{x}}_i \in \mathbb{R}^n$ is the reconstructed (fully sampled) signal represented using the given dictionary $\mathbf{D} \in \mathbb{R}^{n \times k}$ and corresponding “weight” vector $\alpha_i \in \mathbb{R}^k$.

Examples of algorithms capable of solving this include Orthogonal Matching Pursuit (OMP) and its many similar variants^{24,25} or Basis Pursuit, which involves the minimization of the l_1 norm.²⁶

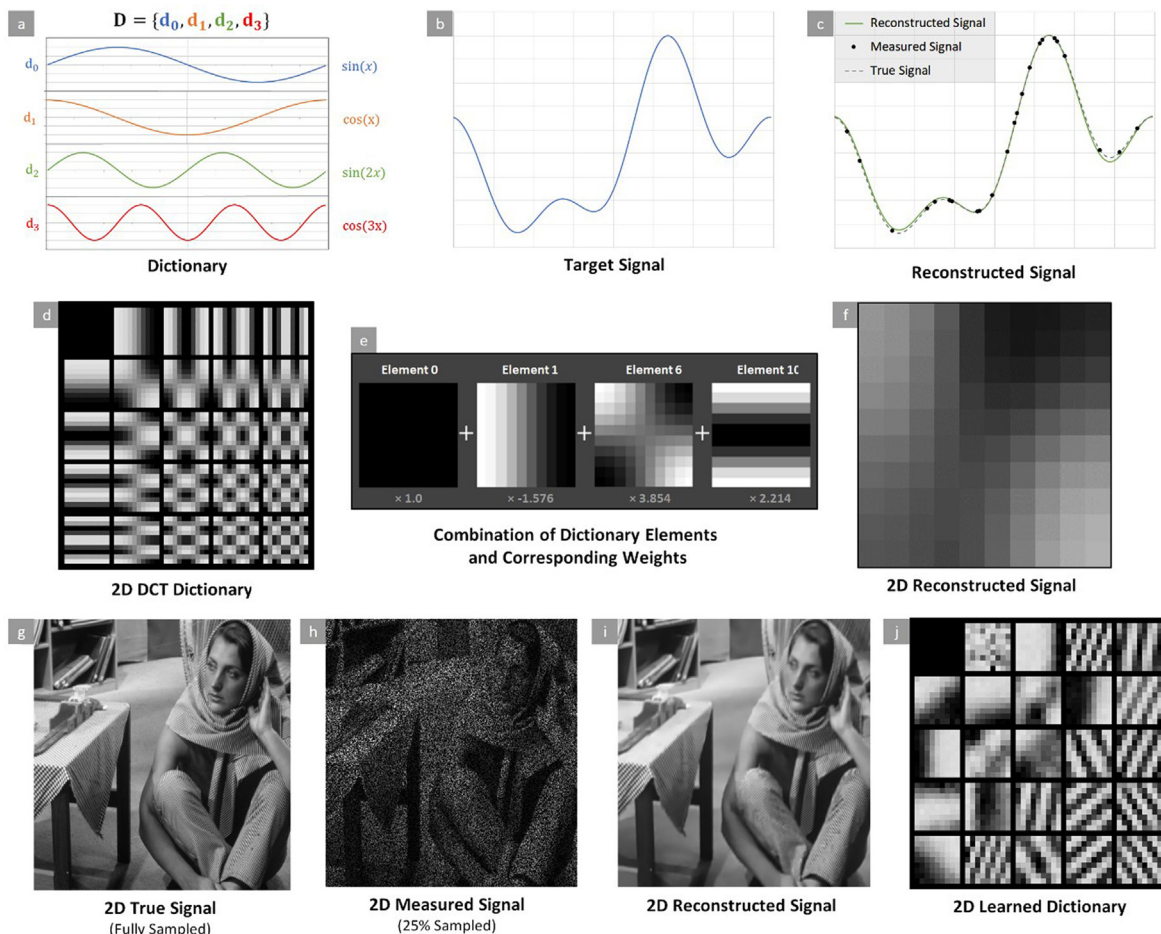


FIG. 2. (a) A series of 1D dictionary elements (Fourier components in this case) can be combined with defined scalar weightings to reproduce the true 1D signal (b). When only a few distinct points in the complex signal are used, it is still possible to generate a good fit using the dictionary elements. (d) A dictionary of 2D elements (again Fourier components) can be combined with defined scalar weightings (e) to produce a reconstruction (f), which is indistinguishable from the true 2D signal. By reducing the number of points in the true signal (g), we can increase the speed and decrease the dose in the sampling of our experiment (h) but still generate a good fit to the data (i). For comparison, (j) shows the dictionary learned directly from the sub-sampled image in (h).

More recently, a reformulation of the dictionary learning problem into the Bayesian regime has produced algorithms, such as Beta-Process Factor Analysis (BPFA),²⁷ which are capable of so-called “blind inpainting,”²⁸ i.e., the formation of a dictionary and subsequent reconstruction of an image using *only* the sub-sampled image as its input (therefore, there is no need for a mask to be provided *a priori* or a fully sampled version of the image to be acquired at any stage in the process). For this reason, BPFA represents an ideal starting algorithm for sub-sampled scanned images, which can be refined using dictionary seeding/transfer approaches (see later Section III of this paper).

As an example of how this process can work, consider the case of a simple one-dimensional (1D) signal, such as a wave shown in Fig. 2. Here, a series of dictionary elements (in this case 1D Fourier components) can be used to reconstruct a true signal [Fig. 2(b)]. However, now what happens if we do not measure the complete signal? Figure 2(c) shows 25% sub-sampling of the true signal from Fig. 2(b). It is clear from Fig. 2(c) that we can fit the dictionary elements to the sub-sampled observation, effectively “inpainting” the missing level of sampling in our experiment. As we reduce the level of sampling, the ability to “fit” to the data with a minimal error is reduced, until typically at $\sim 2\%$ sampling, the error is unacceptably large.²⁹ However, given that the damage induced in the sample is a function of the speed of the scan, the overlap of the beam positions, reducing the overall number of beam positions in the image by this factor of 50, can have a tremendous effect on the overall sample stability during the experiment. This approach is also easily extendable to higher dimension images, with the same approach as above shown for the reconstruction of the 2D image of “Barbara” [Figs. 2(d)–2(i)]. In this case, the reconstruction was obtained using BPFA to Inpaint the sub-sampled image.³⁰

In the use of the BPFA methodology, there are a number of tunable parameters that are used to increase the efficiency of the algorithms to reconstruct the images.¹¹ Here again, it is possible to reconstruct 2D images with high precision from a sampling of $\sim 2\%$ ^{31,32} (this also extends to non-rectangular scans,³³ 3D tomography,^{34,35} 4D methods such as ptychography,^{36,37} and higher dimensional datasets).

III. DICTIONARY TRANSFER AND SEEDING WITH FAST SIMULATIONS

From the results in Sec. II, it is clear that we can use a dictionary for our single sub-sampled image with standard Fourier components or learn the dictionary for the reconstruction directly from the sub-sampled image using BPFA.¹¹ However, could we use a dictionary that we have learned from one image to reconstruct another? The reason we may want to consider this is that if one type of image had a better signal-to-noise ratio (SNR), then we may get a more accurate dictionary, improving the speed and fidelity of the reconstruction of subsequent images if we use the dictionary from that “best image.”³⁰ We may also be able to create a master dictionary that would allow us to sub-select the best dictionary to reconstruct any particular set of images. When using BPFA, which has the benefit of working directly on sub-sampled images, the most time-consuming part of the reconstruction process is the dictionary determination—we can speed up significantly by using an existing optimal dictionary. In order to test this dictionary transfer concept, we can simply try it for two images that show strikingly different contrast and see what happens. Figure 3 shows two images: their dictionaries learnt by K-SVD and the reconstructions of 25% sub-sampled images using the dictionary from the other image. The quality of the reconstructions in each case is shown in Table I. As can be clearly

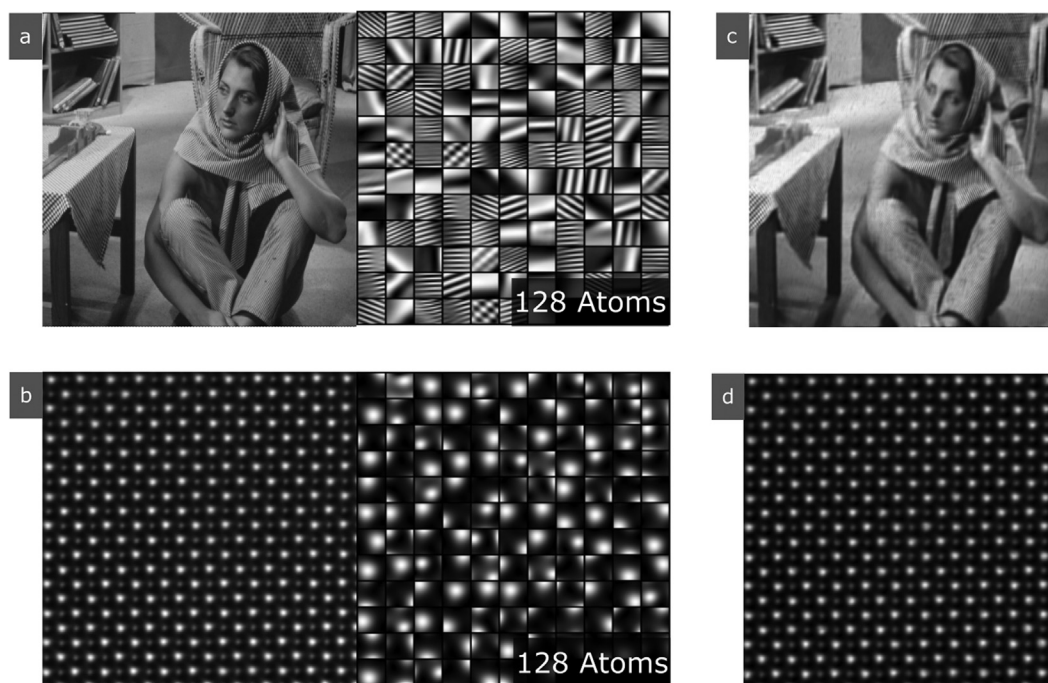


FIG. 3. (a) Image of Barbara and dictionary, (b) atomic resolution STEM image of SrTiO₃ and dictionary, (c) 25% Barbara reconstructed with STEM dictionary, and (d) 25% STEM reconstructed with Barbara dictionary.

seen, it is possible to swap dictionaries and still achieve a high-quality reconstruction. The limitation in this example is that it takes longer to achieve the required reconstruction quality.

A particularly useful application of the dictionary transfer process is in the use of simulations for image analysis. For many types of images in STEM, SEM, and other microscopies, simulations are used to match expected contrast to actual contrast and quantify the structure giving rise to the image. Usually, this is a computationally intensive methodology as the potential unknowns in the image (composition, thickness, detection efficiency, defocus, etc.) require multiple simulations to be performed to match the experimental image.⁴ In the case of the sub-sampling approach, however, we can use the dictionary from a simulated image to seed the experimental reconstruction, or we can use a dictionary learned from experimental image to match the theory, or we can combine the two images together to make a combined dictionary that is optimal for both.³⁴ As we do not need the full dataset for the simulations (BPFA can reconstruct a partial simulation), we can also sub-sample the number of frozen phonon configurations, locations in real space, and experimental conditions to increase the speed for the simulations, potentially allowing for each of them to be performed in real time during experiments.⁴⁰ As with the reconstructions described previously, by having a dictionary and reconstruction, it means that there are quantifiable fits to the experiment, theory, and combination of the two. Rather than matching to experimental conditions, the theory and experiment are solved together, and the differences can be quantified and identified from a single simulation. As a simple example of this approach, 10% sub-sampled simulations of SrTiO₃ obtained using MULTTEM⁴¹ are shown in Fig. 4(a), along with their dictionary and full reconstruction. Also shown in Fig. 4 is the reconstruction of the 25% SrTiO₃ image shown in Fig. 3, using the simulated dictionary in Fig. 4(c). A quantified comparison of the reconstruction of this image is shown in Table I. A key factor here is that unlike the example of Fig. 3, where the dictionary was poorly suited in the transfer and making the reconstruction become more complex, here, we are simplifying the reconstruction by making the dictionary specifically for the experimental image we want to reconstruct.

TABLE I. Comparison of reconstruction quality for the images shown in Figs. 3 and 4 using standard peak signal to noise ratio (PSNR)³⁸ measured in decibels (dB) (the higher the number, the better the reconstruction) and Structural Similarity Index Measure (SSIM)³⁹ metrics (a number closer to 1 is better). As a general rule of thumb, a PSNR value greater than 20 dB is an acceptable reconstruction, over 25 dB is a very good reconstruction, and over 30 dB is indistinguishable from the ground truth (also the same for an SSIM of 0.95 or above). *Note that dictionary generated from image simulation was applied to a cropped area of the full STEM image.

		Input image			
		Barbara		STEM	
		PSNR (dB)	SSIM	PSNR (dB)	SSIM
Dictionary	Barbara	24.72	0.77	25.66	0.9
	STEM	23.81	0.63	31.46	0.98
	Simulation*	26.13	0.92

IV. LEARNING FOR COMPRESSED HYPERSPECTRAL IMAGING

In the discussion so far, we have focused on an approach that uses the dictionary obtained from a single image (and our demonstration example has used atomic resolution images). However, if there are multiple images that are being acquired in an experiment (for example, with a movie and/or multiple different detector types), or we have multiple experiments performed on the same or similar samples, then there are opportunities to refine the reconstruction of sub-sampled images even further. This type of approach falls within the general topic of hyperspectral imaging (HSI),⁴² and there are many powerful deep learning approaches that have been developed for this type of data structure.^{43,44} In the case of their use in scanning (transmission) electron microscopy, the goal in the experiment is always to be ahead of the beam damage that is induced in the experiment, and that means we will always be signal limited and looking for methods that will work under low SNR conditions. In the example we show in this section, we aim to reconstruct a general hyperspectral image data-cube with ten spectral channels and 1 backscattered electron (BSE) channel and avoid the advantages of symmetry that can assist with the reconstruction of atomic resolution images.

Supervised methods^{44,45} make use of a “ground truth” to train a deep neural network (DNN), capable of denoising images, by mapping the noisy image to a clean Ref. 46. This can achieve state-of-the-art image performance with a large enough dataset for training but can struggle to adapt to unseen data with new models of noise. For the STEM case, a ground truth image may not be possible to acquire without damage. However, with unsupervised learning approaches, it is possible for a DNN to instead learn the mapping between independently measured noisy images to predict a clean signal with no reference ground truth,⁴⁷ achieving similar performance to the supervised method. *Noise2Self*⁴⁸ is one method that extended this idea to exploit the noise independence between pixels, relaxing the requirement for collecting two independent noisy images and providing theoretical performance guarantees of such an approach. A semi-supervised approach may also play an important role when there are a ground truth for part of the data.

Figure 5 shows a small section of a much larger area energy dispersive x-ray (EDS) spectrum map acquired with two different dwell times using a scanning electron microscope (SEM). Also shown are reconstructions of these two datasets using a 3D BPFA implementation, in which a high SNR fully sampled backscattered electron (BSE) image is included as one of the layers alongside the EDS data cube. Extended into 3D, rather than learning dictionary elements of size [b × b] as typical with 2D dictionary learning, dictionary elements of size [b × b × N] are used, where N is the number of layers to the data cube (N = 11 for this example). In the case presented, each layer is a different elemental map produced, with the first layer being the BSE image. This dictionary, which considers features along the spectral axis, is designed to take advantage of the relationship that exists between both spatial and spectral information available in the data cube. In using the high signal BSE image, this method aims to take advantage of its high spatial resolution to aid in reconstruction. Two use cases are presented in Fig. 5: a low dwell time acquisition (1 μs), wherein the full spatial domain is sampled, and a high dwell time acquisition (100 μs) in which only 1% of the spatial domain is sampled randomly. These two scenarios exhibit incompleteness in two

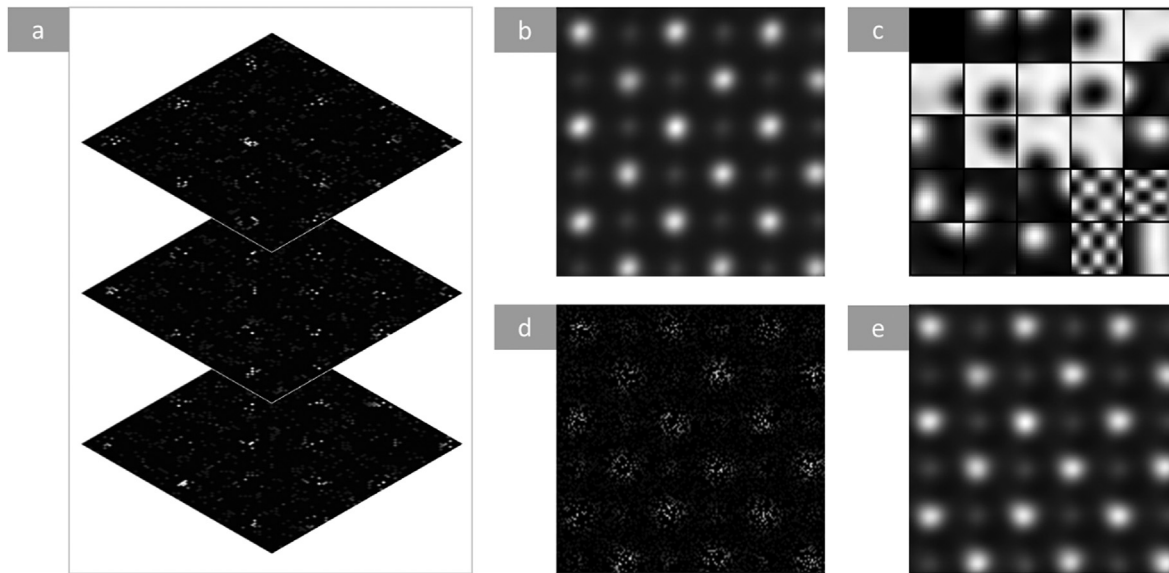


FIG. 4. (a) Three 10% sub-sampled simulations corresponding to different frozen phonon configurations of SrTiO_3 , and the reconstructed simulation using BPFA (b) as well as the dictionary determined by BPFA (c). This dictionary is then used to reconstruct a 25% sub-sampled crop of the SrTiO_3 from Fig. 3(d), with the reconstruction (e) having a 92% similarity to the reference image.

domains: spectral and spatial, respectively. While the low dwell time dataset may sample every location, the spectral information collected at those locations is weak (low SNR). For the high dwell time dataset, the inverse is true; at each sampled location, the full (high SNR) spectra are acquired but only a few datapoints are acquired. 3D BPFA can take both of these inputs and produce detailed spectrum maps with significant quality increases over the original data. Both of these use cases, from an experimental point of view, would theoretically have the same incident electron dose rate and acquisition time. One of the main benefits of using a method such as this is that no training data or prior-learned model is required. All that is necessary is the input data, and a set of input parameters tailored to that input data.

V. CONCLUSIONS AND OUTLOOK

The methodology described here can allow scanned images to be acquired at least 10–100 \times faster and coupled with a dose fractionation that maximizes the beam spacing in space and time, thereby minimizing electron beam damage. Although the full potential of these techniques, such as BPFA and DNN, is yet to be fully exploited and evaluated, such an approach increases the range of beam sensitive samples that can be studied by advanced STEM (and other scanned) methods. In addition, this methodology is particularly important for the rapid throughput of scanned experiments, as technique developments over the last few have moved to more and more pixels over an ever-increasing analysis area. For example, ptychography in STEM,³⁶ serial block face SEM,⁴⁹ and FIB-SEM slice and view⁵⁰ are all pushing large scan dimensions even up to the 100 million pixel range, making the time of image acquisition the main limitation that is key to all future applications of these methods. In some cases, such as Z-contrast STEM,⁴ by reducing the number of pixels in an image, dynamic *in situ* phenomena can be directly observed where the beam does not significantly change the observation.⁵¹ Techniques that were once only

thought of as only applicable to high resolution imaging can, therefore, now become *in situ* methods. The use of DNNs to learn an Inpainting model from a set of samples means that we can also, in principle, teach a microscope how to image a particular type of sample more efficiently.

Another aspect of scanned imaging is that this form of sub-sampling and Inpainting reconstruction facilitates is the potential for dynamic control of the microscope. If we take a 1 mega pixel example with a 1 μs dwell time, then on a standard scan, we would acquire ~ 1 frame per second (not accounting for the flyback time). At 10% sampling, this becomes 10 frames/second, which means that we effectively can perform sub-original-frame analysis for key things like defocus, stigmatism, drift, tilt, etc., or measure damage and damage rate independently to determine the best acquisition time for high resolution images. While the ability to reconstruct the image and perform the analytics to change the microscope alignment parameters would have to be performed in real time, there is increasing evidence that this should be routinely possible soon. The codes that perform the Inpainting work on a patch-by-patch basis across the whole image and each refinement can be performed in parallel, meaning that the speed can be increased by scaling efficient codes on a GPU platform. The difference in time between the Inpainting of a 5% sampled image and a 10% sampled image is negligible, meaning that the final speed of the imaging process is limited only by the acquisition time at these sampling levels. For things like defocus and drift, it is also important to understand that we also do not need to reconstruct across the whole image to accomplish control, and a few patches at specific locations would be all that would be needed. Another key part of the speed discussion is that there is a difference between the image that is needed to control the microscope and the image that is used for the final analysis. A poorer quality, i.e., faster reconstruction, could be enough to control the microscope and ensure that the best experimental imaging

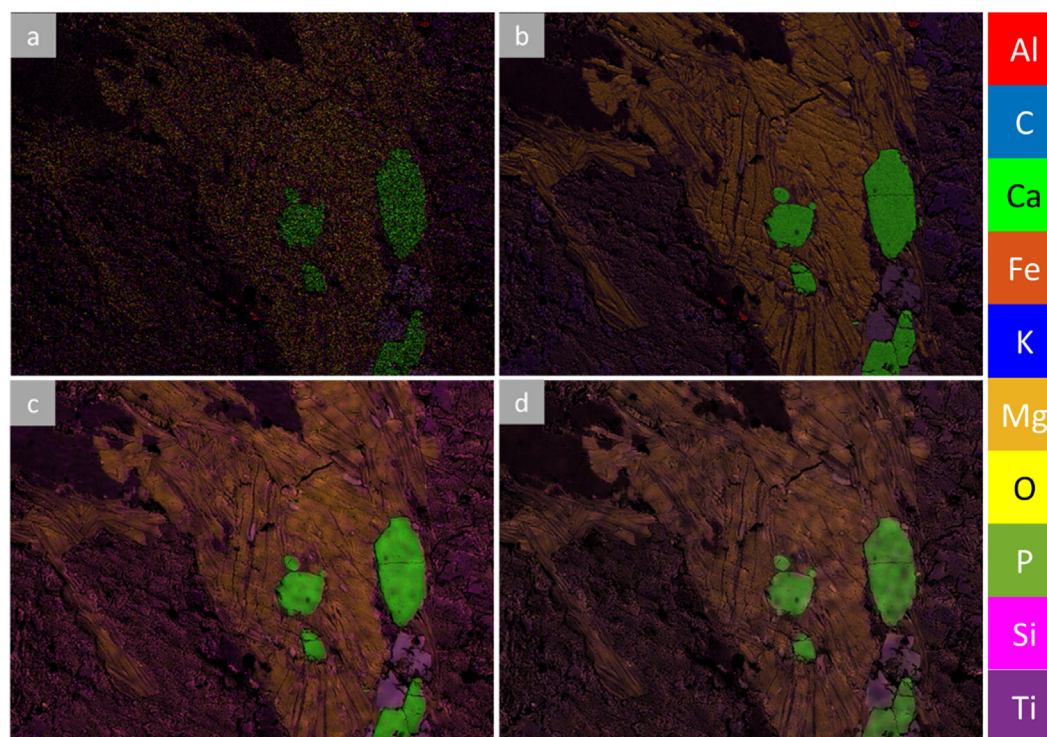


FIG. 5. (a) Untreated EDS spectrum image with 1 μ s dwell time at 100% sampling from a sample of granite, containing the following minerals: muscovite (purple), illite (orange), quartz (dark purple), apatite (green), and rutile (lilac). (b) Untreated EDS spectrum image with 100 μ s dwell time at 100% sampling. (c) 3D BPFA treated version of (a), 1 μ s dwell time at 100% sampling. (d) 3D BPFA treated version of (b), with 100 μ s dwell time but sampled randomly at 1%. Both (c) and (d) have the same theoretical electron dose exposure and acquisition time. Changes in image contrast between (a) and (b) are due to increased signal-to-noise ratio when scanning with higher dwell times. Changes in image contrast between (c) and (d), which are formed from the same electron dose rate, are due to the efficiency of the algorithm to construct the complete dataset. All images contain the BSE image as a layer in the data cube. Image color denotes chemical composition, as indicated by the legend. Image dimensions are $1.11 \times 0.835 \text{ mm}^2$. We would like to thank Dr Louise Hughes and Dr Matthew Hiscock for supplying these data and help with analysis.

parameters were used during the experiment. After the experiment is completed, all the images could be transferred and analyzed with a range of dictionaries, algorithms, and approaches to determine the best result after the optimal reconstruction methods were used. Of course, at this point, the best overall result would then be used to modify the dictionary/algorithm in a positive way, allowing all previous images to be re-analyzed to improve existing/prior results.

It is worth noting that all of the above discussions for the use of the data are with images that are $\sim 1\%$ – 10% of the size of the original fully sampled image. At the time of acquisition, whatever the best approach to reconstruction exists would set the limit of sub-sampling and ensure that there is no data loss ever. Improvements in reconstruction and analysis that may come from a better algorithm in the future are not inherent in the storage architecture, meaning that the smallest amount of data is always kept for the best algorithm available—a better algorithm may lead to all existing images being reduced even further. Another key part in the discussion of scanned images is that often it is not the image that is important but the analysis of what the image shows, for example, the number and size distribution of nanoparticles in a particular area or part of the structure. As there is enough information in the sub-sampled image to reconstruct a full image, it means there is enough information to work with advanced image analytics. So, in the example

above, the image analytics for edge detection and size determination would be able to run directly on the sub-sampled data, but as it is sub-sampled, there is less data to analyze and a faster result.^{52,53} It may be possible that complete data analysis could be performed during a microscope experiment, and users of the instruments leave with their data rather than their results to be analyzed at a later time. As with the final resolution of the images, even if there are sacrifices in having large error bars in data to get it quickly, the quality of data will be enough to determine the course of the experiment, and the errors can always be improved off-line using the best supporting data/algorithms.

In summary, whether sub-sampling and inpainting are used to improve image speed, control dose fractionation, reduce damage, provide real time adaptive scanning and autonomous instrument controls, learn the optimal reconstruction and denoising approach to all (sub- and fully sampled) images, or simply to reduce size of images for storage and/or transmission, these applications can all fundamentally change the way that we acquire and use images from STEM and other scanned microscopes in the future.

This work was performed in the Albert Crewe Centre (ACC) for Electron Microscopy, a shared research facility (SRF) fully supported by the University of Liverpool. This work was also

funded by the EPSRC Centre for Doctoral Training in Distributed Algorithms (EP/S023445/1) and by Sivananthan Laboratories.

AUTHOR DECLARATIONS

Conflict of Interest

The authors have no conflicts to disclose.

Author Contributions

Nigel D. Browning: Conceptualization (equal); Data curation (equal); Investigation (equal); Methodology (equal); Project administration (equal); Supervision (equal); Writing – original draft (equal); Writing – review & editing (equal). **Jony Castagna:** Conceptualization (equal); Project administration (equal); Supervision (equal); Writing – original draft (equal); Writing – review & editing (equal). **Angus I. Kirkland:** Funding acquisition (equal); Supervision (equal); Writing – review & editing (equal). **Amirafshar Moshaghpour:** Funding acquisition (equal); Investigation (equal); Methodology (equal); Supervision (equal); Validation (equal); Writing – review & editing (equal). **Daniel Nicholls:** Data curation (equal); Investigation (equal); Methodology (equal); Supervision (equal); Validation (equal); Writing – review & editing (equal). **Jack Wells:** Data curation (equal); Investigation (equal); Methodology (equal); Software (equal); Writing – review & editing (equal). **Alex W. Robinson:** Data curation (equal); Investigation (equal); Methodology (equal); Software (equal); Validation (equal); Writing – review & editing (equal). **Yalin Zheng:** Data curation (equal); Investigation (equal); Methodology (equal); Supervision (equal); Validation (equal); Writing – review & editing (equal).

DATA AVAILABILITY

The data that support the findings of this study are available within the article.

REFERENCES

- ¹X. Sang, A. R. Lupini, R. R. Unocic, M. Chi, A. Y. Borisevich, S. V. Kalinin, E. Endeve, R. K. Archibald, and S. Jesse, *Adv. Struct. Chem. Imag.* **2**, 6 (2016).
- ²X. Sang, A. R. Lupini, J. Ding, S. V. Kalinin, S. Jesse, and R. R. Unocic, *Sci. Rep.* **7**, 43585 (2017).
- ³S. J. Pennycook and P. D. Nellist, *Scanning Transmission Electron Microscopy: Imaging and Analysis* (Springer Science & Business Media, 2011).
- ⁴P. E. Batson, N. Dellby, and O. L. Krivanek, *Nature* **418**, 617 (2002).
- ⁵R. F. Egerton, *Ultramicroscopy* **127**, 100 (2013).
- ⁶A. Stevens, H. Yang, L. Carin, I. Arslan, and N. D. Browning, *Microscopy* **63**(1), 41 (2014).
- ⁷L. Kovarik, A. Stevens, A. Liyu, and N. D. Browning, *Appl. Phys. Lett.* **109**(16), 164102 (2016).
- ⁸A. Stevens, L. Luzi, H. Yang, L. Kovarik, B. L. Mehdi, A. Liyu, M. E. Gehm, and N. D. Browning, *Appl. Phys. Lett.* **112**(4), 043104 (2018).
- ⁹D. Nicholls, J. Lee, H. Amari, A. J. Stevens, B. L. Mehdi, and N. D. Browning, *Nanoscale* **12**(41), 21248 (2020).
- ¹⁰D. Nicholls, J. Wells, A. Stevens, Y. Zheng, J. Castagna, and N. D. Browning, *Ultramicroscopy* **233**, 113451 (2022).
- ¹¹A. Velazco, A. Béché, D. Jannis, and J. Verbeeck, *Ultramicroscopy* **232**, 113398 (2022).
- ¹²D. Jannis, A. Velazco, A. Béché, and J. Verbeeck, *Ultramicroscopy* **240**, 113568 (2022).
- ¹³A. Ishizuka, M. Hytch, and K. Ishizuka, *Microscopy* **66**, 217–221 (2017).
- ¹⁴K. Reidy, G. Varnavides, J. D. Thomsen, A. Kumar, T. Pham, A. M. Blackburn, P. Anikeeva, P. Narang, J. LeBeau, and F. M. Ross, *Nat. Commun.* **12**, 1290 (2021).
- ¹⁵X. Ke, M. Zhang, K. Zhao, and D. Su, *Small Methods* **6**, 2101040 (2022).
- ¹⁶D. L. Donoho, *IEEE Trans. Inform. Theory* **52**(4), 1289 (2006).
- ¹⁷E. J. Candès, J. Romberg, and T. Tao, *IEEE Trans. Inform. Theory* **52**(2), 489 (2006).
- ¹⁸K. Kreutz-Delgado, J. F. Murray, B. D. Rao, K. Engan, T. W. Lee, and T. J. Sejnowski, *Neural Comput.* **15**(2), 349 (2003).
- ¹⁹R. G. Baraniuk, *IEEE Signal Process. Mag.* **24**(4), 118 (2007).
- ²⁰M. Bertalmio, G. Sapiro, V. Caselles, and C. Ballester, paper presented at the Proceedings of the 27th Annual Conference on Computer Graphics and Interactive Techniques, 2000.
- ²¹M. Fornasier and H. Rauhut, *Handbook of Mathematical Methods in Imaging* (Springer, 2015).
- ²²K. Engan, S. O. Aase, and J. H. Husoy, paper presented at the IEEE International Conference on Acoustics, Speech, and Signal Processing (ICASSP99), 1999.
- ²³M. Aharon, M. Elad, and A. Bruckstein, *IEEE Trans. Signal Process.* **54**(11), 4311 (2006).
- ²⁴D. Needell and R. Vershynin, *Found. Comput. Math.* **9**(3), 317 (2009).
- ²⁵D. Needell and J. A. Tropp, *Appl. Comput. Harmonic Anal.* **26**(3), 301 (2009).
- ²⁶S. Chen and D. Donoho, paper presented at the Proceedings of 28th Asilomar Conference on Signals, Systems and Computers, 1994.
- ²⁷J. Paisley and L. Carin, paper presented at the Proceedings of the 26th Annual International Conference on Machine Learning, 2009.
- ²⁸S. Sertoglu and J. Paisley, paper presented at the 23rd European Signal Processing Conference (EUSIPCO), 2015.
- ²⁹D. Nicholls, A. Robinson, J. Wells, A. Moshaghpour, M. Bahri, A. Kirkland, and N. Browning, paper presented at the IEEE International Conference on Acoustics, Speech and Signal Processing (ICASSP), 2022.
- ³⁰J. Wells, D. Nicholls, A. Robinson, Y. Zheng, J. Castagna, and N. D. Browning, “Dictionary transfer and cross-compatibility in dictionaries for image inpainting” (unpublished).
- ³¹A. Zobelli, S. Y. Woo, A. Tararan, L. H. G. Tizei, N. Brun, X. Li, O. Stephan, M. Kociak, and M. Tence, *Ultramicroscopy* **212**, 112912 (2020).
- ³²J. M. Ede and R. Beanland, *Sci. Rep.* **10**, 8332 (2020).
- ³³X. Li, O. Dyck, S. V. Kalinin, and S. Jesse, *Microsc. Microanal.* **24**, 623–633 (2018).
- ³⁴Z. Saghi, B. Winter, R. Leary, E. Spiecker, C. Ducati, and P. Midgley, *Ultramicroscopy* **160**, 230–238 (2016).
- ³⁵R. Leary, Z. Saghi, P. A. Midgley, and D. J. Holland, *Ultramicroscopy* **131**, 70 (2013).
- ³⁶J. M. Rodenburg, *Adv. Imaging Electron Phys.* **150**, 87–184 (2008).
- ³⁷A. Stevens, H. Yang, W. Hao, L. Jones, C. Ophus, P. D. Nellist, and N. D. Browning, *Appl. Phys. Lett.* **113**(3), 033104 (2018).
- ³⁸A. Horé and D. Ziou, *IET Image Process.* **7**, 12–24 (2013).
- ³⁹Z. Wang, A. C. Bovik, H. R. Sheikh, and E. P. Simoncelli, *IEEE Trans. Image Process.* **13**, 600–612 (2004).
- ⁴⁰A. W. Robinson, D. Nicholls, J. Wells, A. Moshaghpour, A. Kirkland, and N. D. Browning, *Ultramicroscopy* **242**, 113625 (2022).
- ⁴¹I. Lobato and D. Van Dyck, *Ultramicroscopy* **156**, 9–17 (2015).
- ⁴²J. M. Bioucas-Dias, A. Plaza, N. Dobigeon, M. Parente, Q. Du, P. Gader, and J. Chanussot, *IEEE J. Sel. Top. Appl. Earth Obs. Remote Sens.* **5**(2), 354 (2012).
- ⁴³O. Sidorov and J. Y. Hardeberg, paper presented at the Proceedings of the IEEE/CVF International Conference on Computer Vision Workshops, 2019.
- ⁴⁴R. Wong, Z. Zhang, Y. Wang, F. Chen, and D. Zeng, *IEEE J. Sel. Top. Appl. Earth Obs. Remote Sens.* **13**, 4369 (2020).
- ⁴⁵C. Tian, L. Fei, W. Zheng, Y. Xu, W. Zuo, and C. W. Lin, *Neural Networks* **131**, 251 (2020).
- ⁴⁶X. Mao, C. Shen, and Y. B. Yang, in Proceedings of the 30th International Conference on Neural Information Processing Systems, 2016.
- ⁴⁷J. Lehtinen, J. Munkberg, J. Hasselgren, S. Laine, T. Karras, M. Aittala, and T. Aila, *arXiv:1803.04189* (2018).
- ⁴⁸J. Batson and L. Royer, paper presented at the International Conference on Machine Learning, 2019.
- ⁴⁹W. Denk and H. Horstmann, *PLoS Biol.* **2**(11), e329 (2004).
- ⁵⁰L. Holzer, F. Indutnyi, P. H. Gasser, B. Münch, and M. Wegmann, *J. Microsc.* **216**(1), 84 (2004).
- ⁵¹B. L. Mehdi, A. Stevens, L. Kovarik, N. Jiang, H. Mehta, A. Liyu, S. Reehl, B. Stanfill, L. Luzi, and W. Hao, *Appl. Phys. Lett.* **115**(6), 063102 (2019).
- ⁵²S. Reehl, B. Stanfill, M. Johnson, D. Ries, N. D. Browning, B. L. Mehdi, and L. Bramer, *Qual. Eng.* **32**(2), 244 (2020).
- ⁵³B. A. Stanfill, S. M. Reehl, M. C. Johnson, N. D. Browning, B. L. Mehdi, P. C. Caragea, and L. M. Bramer, *ChemCatChem* **10**(14), 3115 (2018).